ACS APPLIED MATERIALS & INTERFACES

Research Article

www.acsami.org

Improved Oxygen Reduction Reaction Catalyzed by Pt/Clay/Nafion Nanocomposite for PEM Fuel Cells

B. Narayanamoorthy,[†] K. K. R. Datta,[‡] M. Eswaramoorthy,[‡] and S. Balaji*,[†]

[†]Department of Chemistry, Faculty of Science, Sri Chandrasekharendra Saraswathi Viswa Mahavidyalaya (SCSVMV University), Enathur, Kanchipuram - 631 561, India

[‡]Nanomaterials and Catalysis Lab, Chemistry and Physics of Materials Unit, Jawaharlal Nehru Centre for Advanced Scientific Research (JNCASR), Bangalore - 560 064, India

Supporting Information

ABSTRACT: A novel Pt nanoparticle (Pt NP) embedded aminoclay/Nafion (Pt/AC/N) nanocomposite catalyst film was prepared for oxygen reduction reaction by sol−gel method. The prepared nanocomposite films were surface characterized using XRD and TEM and thermal stability was studied by TGA. The prepared film has firmly bound Pt NP and could exhibit an improved electro-reduction activity compared to vulcan carbon/Nafion supported Pt NP (Pt/VC/N). Moreover, the Pt/AC/N film possessed good stability in the acidic environment. The limiting current density of the Pt/AC/N film with 35.4 $\mu g/cm^2$ of Pt loading was found to be 4.2 mA/cm^2, which is 30% higher than that of the Pt/VC/N. The maximum H_2O_2 intermediate formation was found to be ∼1.6% and the reaction found to follow a four electron transfer mechanism. Accelerated durability test for 2000 potential cycles showed that ca. 78% of initial limiting current was retained. The results are encouraging for possible use of the Pt/AC/N as the free-standing electrocatalyst layer for polymer electrolyte membrane fuel cells.

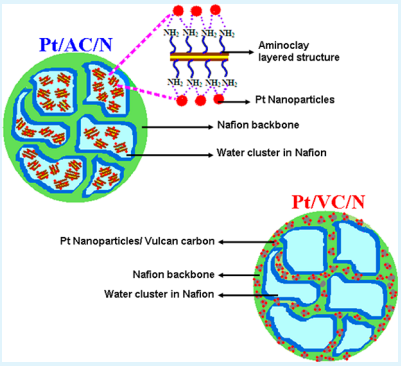

KEYWORDS: *PEM fuel cells, oxygen reduction reaction, aminoclay/Nafion nanocomposite, cyclic voltammetry*

1. INTRODUCTION

Fuel cells are electrochemical energy conversion systems with higher thermodynamic efficiency than internal combustion engines and one of the promising sources of clean energy.[1−5] Among various types of fuel cells, polymer electrolyte membrane (PEM) fuel cells are highly attractive due to the ambient temperature working conditions, high specific power density, quick startup, and easy portability.[6−9] However, the higher cost and the poor efficiency of the cathode catalyst for oxygen reduction reaction (ORR) throw some technical challenges to make it a commercially viable process.[10] The oxygen reduction process involves the breaking of an O−O bond and the formation of an O−H bond which requires metal surfaces that strongly enhance the kinetics of bond-breaking and bond-forming steps.[11,12] The most widely used catalyst for ORR is Pt due to its high catalyzing nature, anticorrosive properties, and high stability[13−15] and is usually supported on carbon based materials (Pt/C) due to the unique properties of carbon such as high surface area availability, conductivity, porous structure, and so forth. Despite its widespread use, carbon support is known to undergo electrochemical oxidation to CO_2 at the cathode of a fuel cell, thereby reducing the Pt surface activity due to agglomeration of Pt nanoparticles (Pt NP), and many studies have reported decreased performance of the Pt/C catalyst due to agglomeration and loss of Pt NP content due to carbon surface corrosion.[16−19]

In order to avoid corrosion of carbon support, other alternative support materials, namely, natural or synthetic clays, have been used.[20,21] Zhang et al. have reported the chemical vapor deposition of Pt NP over Cloisite 20A clay (Pt/clay) and fabrication of the Pt/clay over Nafion to obtain catalyst membrane for use in PEM fuel cells. They have observed an increase in current density with Pt/clay/N catalyst membrane compared to pure Nafion membrane.[22] Premkumar and Ramaraj have studied the reduction of dioxygen using Pt deposited over bentonite clay/Nafion coated electrode.[23] The improved barrier properties of clay/Nafion composite membranes for PEM fuel cell applications have been reported.[24−27] Jung et al. have investigated the barrier properties of montmorillonite clay (MMT)/Nafion membrane for methanol permeation in direct methanol fuel cells and found a little reduction in methanol permeation.[28] However, the absence of functional groups on MMT limits the uniform distribution of metal nanoparticles. Naturally occurring clays are subjected to surface modification for better intercalation with polymers to form nanocomposites.[29−31] MMT type of clays requires surface modification, and also these modified clays are more soluble in organic medium, restricting their usage in aqueous medium.

Received: April 20, 2012
Accepted: July 3, 2012
Published: July 3, 2012

Nafion ionomer is widely used for the fabrication of membrane electrode assembly in PEM fuel cell stack systems and used as binder material in characterizing the catalyst layers in a three electrode configuration cell to keep the catalyst particles intact. It is well documented that Nafion contains heavily interconnected water channels of diameter ca. 4.0 nm formed through self-aggregation of sulfonic acid groups.[32] Therefore, clay with surface functionality for binding Pt NP may be used with Nafion to form stable catalyst layers. For better interaction of hydrophilic domains of Nafion, water dispersible clay will be highly desirable and can efficiently bind to metal nanoparticles. The synthetic "amino group functionalized Mg−phyllosilicate clay" (briefly aminoclay) is one such water dispersible clay and also can effectively bind to metal nanoparticles.[33] Aminoclay (AC) during the exfoliation process goes to single or few layer sheets[33] which can in principle have nice binding toward hydrophilic domains of Nafion. Thus, AC containing surface functionality may serve as a good support, and the uniform distribution of metal nanoparticles could be achieved due to the presence of AC over Nafion matrix. Datta et al. have reported the stabilization of Ag, Au, Pd, and Pt NP over AC[33] and also studied the permselective nature of the AC toward Cu NP which selectively allows only the ions to pass through it and AC-PVA nanocomposites exhibiting good oxygen barrier and improved ductile properties compared to neat PVA.[34,35] These remarkable properties of AC could be harnessed if suitably incorporated with Nafion for holding Pt NP and for catalyzing ORR.

Here, we report for the first time the fabrication and electrochemical characterization of Pt NP embedded AC/Nafion nanocomposite films (Pt/AC/N) which exhibit good oxygen reduction activity compared to the Pt/vulcan carbon/Nafion (Pt/VC/N) nanocomposite films in acid medium. The prepared catalyst films were surface characterized using transmission electron microscope (TEM), X-ray diffraction (XRD), and thermal gravimetric analysis (TGA) analyses. The effect of accelerated potential cycling on ORR kinetics was investigated, and the mechanistic pathway is presented.

2. EXPERIMENTAL SECTION

Materials. 3-Aminopropyltriethoxysilane ($C_9H_{23}NO_3Si$, Sigma), $MgCl_2.6H_2O$, chloroplatinic acid hexahydrate (Sigma), sodium borohydride (Rankem), Nafion perfluorinated polymer resin solution (5 wt %, Aldrich), sulfuric acid (Rankem), absolute ethanol (s.d. fine), and *N*,*N*′-dimethylformamide (Rankem) were used as received. Vulcan XC-72 carbon was received as a gift sample from Cabot (I) Ltd.

Methods. The AC was prepared by the method reported in the literature.[36] Typically, an AC was prepared at room temperature by dropwise addition of 3-aminopropyltriethoxysilane (1.3 mL, 5.85 mmol) to an ethanolic solution (20 g) of magnesium chloride (0.84 g, 3.62 mmol). The white slurry obtained after 5 min was stirred overnight and the precipitate isolated by centrifugation, washed with ethanol (20 mL), and dried at 50 °C in air. H_2PtCl_6 was used as metal precursor for the preparation of Pt nanoparticles. The synthesized AC was then exfoliated by dispersing 20 mg of clay in 2 mL of Millipore water by sonication for 2 min. To this transparent clay suspension 2 mL of 1 mM H_2PtCl_6 solution was added followed by the slow addition of 2 mL of 0.1 M of $NaBH_4$ solution. Pt/AC/N nanocomposite membranes were prepared by solvent recasting procedure as follows. A desired amount of Pt/AC from the previous stage was mechanically mixed into deionized water. Then a mixture of 5 wt % Nafion solution, DMF, and ethanol with a volume ratio of 2:1:1 was added to the aqueous mixture of Pt/AC, and the whole mixture was sonicated using an ultrasonication bath at room temperature for 10 min. This mixture was then stirred at 95 °C until a gel-like solution was obtained. The high viscous mixture was cast onto a working electrode area (disk of rotating ring disk electrode (RRDE)) or glass Petri dish and dried at room temperature slowly and then at 80 °C in a nonconvection air oven for 2 h. The clay loading inside the nanocomposite membrane was varied from 2 to 10 wt % with respect to Nafion and Pt mass loading was varied from 18.2 $\mu g/cm^2$ to 209.2 $\mu g/cm^2$ of the GC disk area (0.2471 cm^2). For comparison of ORR activities, Pt/VC/N was prepared following the same procedure as above. Briefly, to a 2 mL solution of 20 mg VC, 2 mL of 1 mM H_2PtCl_6 solution was added followed by the slow addition of 2 mL of 0.1 M of $NaBH_4$ solution. Pt/VC/N nanocomposite membranes were prepared by solvent recasting procedure similar to the procedure shown above for Pt/AC/N.

Characterization Techniques. ATR-FTIR spectra were recorded for AC and Pt/AC/N film using Bruker FTIR spectrometer (Alpha). Powder XRD patterns were recorded using Bruker-D8 diffractometer using Cu Kα radiation, (λ = 1.54 Å, step size: 0.02, current: 30 mA, and voltage: 40 kV), and the mean nanoparticle size was calculated by applying the Debye−Scherrer equation. For TEM analysis, the sample was redispersed in absolute ethanol by sonication before drop casting on a carbon-coated copper grid. TEM measurement was recorded on a JEOL JEM-3010 electron microscope with an applied acceleration voltage of 300 kV. TGA was performed using Mettler-Toledo 850 from 30 to 800 °C in nitrogen atmosphere at a heating rate of 10 °C per minute. The electrochemical measurements were conducted to investigate the catalytic activity of the Pt/AC/N nanocomposite films for ORR in acidic medium. RRDE measurements were performed in 0.5 M H_2SO_4 solution in a three electrode double walled thermostated cell. A 0.2 mm platinum sheet (1 cm^2) was used as the counter electrode and a thin gap RRDE taken as the working electrode (Pine) while the reference electrode used was double junction Ag/AgCl in 3 M KNO_3 (Pine). The working electrode was polished to a mirror finish using 0.05 μm alumina slurry (Buehler) prior to each catalyst coating. The GC disk of the RRDE working electrode was loaded with an aliquot of 15 μL of the prepared colloidal catalyst ink and allowed to dry in N_2 atmosphere. For convenience all potentials are reported relative to the reversible hydrogen electrode (RHE), and current density was calculated using the GC disk area. The static and hydrodynamic voltammetry experiments were conducted with a computer interfaced bipotentiostat (Autolab PGSTAT-128N) controlled by Nova 1.6 software in conjunction with a rotator (Pine). Voltammetric studies were carried out after nitrogen or oxygen purging for 15 min before start of the experiment and forming a blanket during the experiment. Prior to each voltammetry, the potential cycling was carried out in the potential window 0.0−1.2 V vs RHE. Blank cyclic voltammetry (CV) experiments were conducted in N_2 purged 0.5 M H_2SO_4 to calculate electrochemically active surface area (ECSA). The ring currents were measured keeping the constant ring potential of 1.2 V vs RHE, where the oxidation of peroxide is diffusion limited and such potential is sufficiently high to enable the complete oxidation of any H_2O_2 reaching the ring by centrifugal flow due to the rotation. The formation of H_2O_2 intermediate can be calculated from the ring and disk currents and the equation used to calculate the percentage of H_2O_2 is given as follows:[37]

$$H_2O_2\ (\%) = \frac{2I_R/N}{I_D + I_R/N} \times 100$$

where I_D is the disk current, I_R is the ring current, and N is the RRDE collection efficiency ($N = -I_R/I_D$). The collection efficiency for the RRDE electrode used was estimated to be 0.37[38] from the experimental values of I_R and I_D using the classical redox couple $[Fe(CN)_6]^{3-}/[Fe(CN)_6]^{4-}$ in 1 M KNO_3.

The corrosion behavior was tested by chronoamperometry in an airtight three electrode electrochemical cell at 0.7 V vs RHE, and the evolved CO_2 was measured quantitatively (ppmv) using an infrared CO_2 gas analyzer (Geotechnical Instruments, Anagas, CD 95). For accelerated durability, test potential cycling was carried out between

0.2 and 1.2 V vs RHE at the scan rate of 50 mV/s in O_2-purged 0.5 M H_2SO_4 solution at 25 °C.

3. RESULTS AND DISCUSSION

The approximate unit cell composition of AC is $R_8Si_8Mg_6O_{16}(OH)_4$ (R = $CH_2CH_2NH_2$) and consisted of octahedrally coordinated MgO/OH sheets (brucite) overlaid on both sides with a tetrahedrally coordinated aminopropyl-functionalized silicate network as a layered structure.[39] An important feature of AC is its free and immediate exfoliation in water due to the protonation of amine groups.[33] The schematic diagrams for Pt/AC/N and Pt/VC/N are shown in Figure 1.

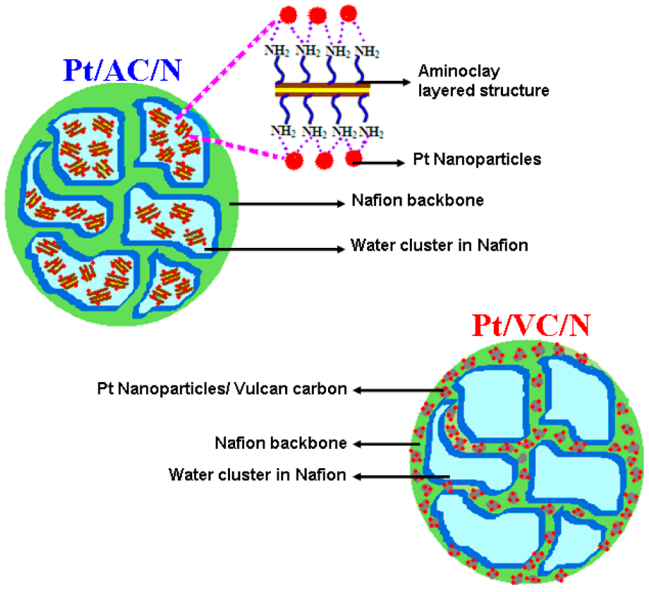

Figure 1. Schematic representation of Pt NP embedded over AC/Nafion and VC/Nafion nanocomposite.

ATR-FTIR spectra (see the Supporting Information, SI-1) for AC and Pt/AC/N were recorded. The symmetric stretching and bending frequencies for the amino group were seen respectively in the range 3500−3400 cm^{-1} and 1650−1550 cm^{-1} confirming the presence of $-NH_2$ group. XRD patterns of AC, AC/N, and Pt/AC/N are shown in Figure 2. The as-synthesized AC exhibits a basal distance of 1.6 nm at 2θ = 5.5°, along with broad in-plane peaks at 2θ = 22 and 35° with corresponding d-spacing of 0.4 and 0.25 nm, respectively. The characteristic peak around 2θ = 60° corresponding to the 2:1 trioctahedral smectite clay is weak due to the stacking disorder induced by the organofunctional groups (Figure 2a). The absence of the d_{001} peak at 2θ = 5.5° corresponding to the AC in the AC/N and Pt/AC/N nanocomposites confirms the extensive exfoliation of clay within the Nafion polymer (Figure 2b,c). On the other hand, Nafion possesses a broad peak centered at 2θ = 17° due to its semicrystalline nature.[40] This peak position is retained even after the stabilization of Pt NP ,indicating the structural integrity of the Nafion network. Furthermore, we observe a broad (111) reflection centered at 2θ = 39° corresponding to the face centered cubic structure of crystalline Pt. This peak is very broad and weak, suggesting the formation of nanocrystalline Pt within the AC/N matrix. This is further evident from the TEM image, showing less than 5 nm sized Pt NP (dark spherical dots) homogenously distributed over the AC/N matrix (Figure 3a). In the case of the Pt/VC/N composite, we observe mostly fused Pt NP (as compared to that of Pt/AC/N) on the back drop of VC/N matrix (Figure 3b). The uneven distribution and coalescence of Pt NP in the case of Pt/VC/N composite is due to the absence of functional groups in VC as compared to that of AC. The TGA images of pristine Nafion, AC/N, Pt/AC/N, and Pt/VC/N are presented

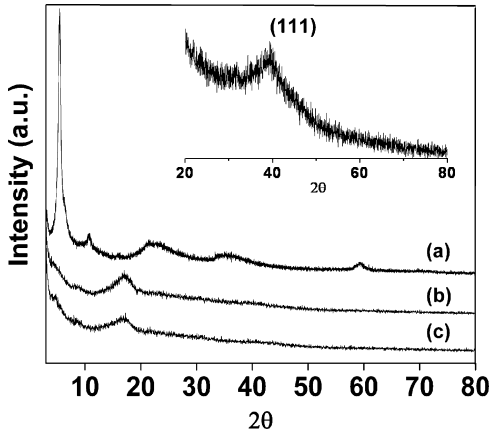

Figure 2. XRD patterns of (a) AC, (b) 6 wt % AC/Nafion nanocomposite, and (c) Pt NP (10 wt %) embedded AC/N nanocomposite, inset showing the (111) peak corresponding to Pt NP.

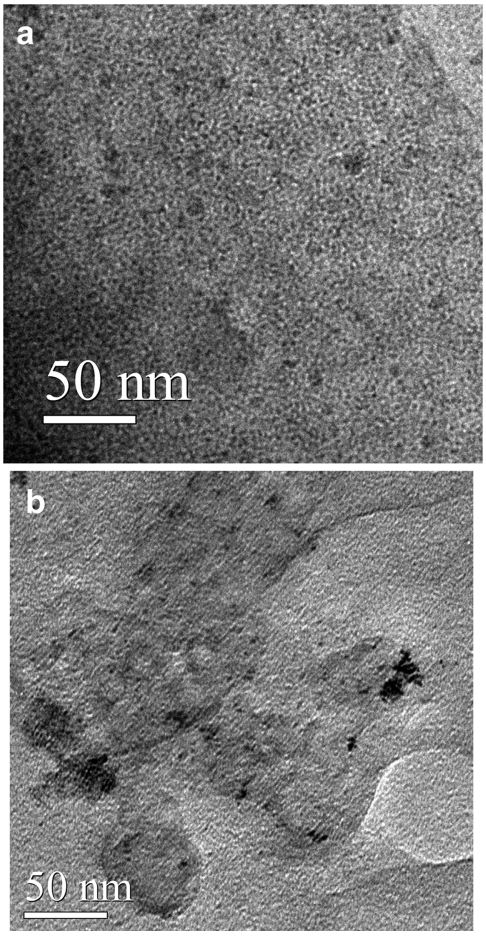

Figure 3. Transmission electron microscope images for Pt NP (170 μg) embedded over (a) 6 wt % AC/Nafion and (b) 6 wt % VC/Nafion matrixes.

dx.doi.org/10.1021/am300697q | ACS Appl. Mater. Interfaces 2012, 4, 3620−3626

in Figure 4. The thermal stability of Nafion slightly increases after the incorporation of 6 wt % of AC. This is due to the

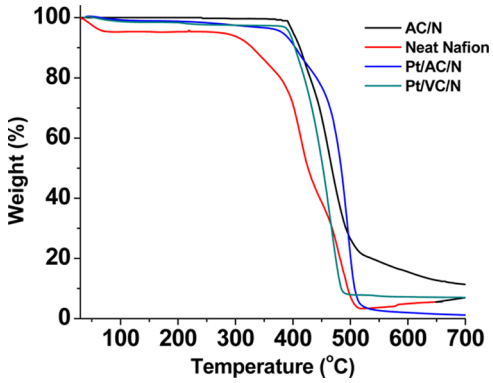

Figure 4. TGA curves for neat Nafion, 6 wt % AC/N nanocomposite, Pt NP (170 μg) embedded over AC, and VC Nafion matrix.

extensive exfoliation of individual AC platelets over the Nafion network. Furthermore, there is no significant change in the thermal stability of Pt/AC/N and Pt/VC/N films, and it is comparable to that of the AC/N nanocomposites.

Figure 5a shows the CVs of Pt/AC/N in N_2 purged 0.5 M H_2SO_4 solution at the scan rate of 50 mV/s at 25 °C recorded in the potential range −0.1 V and +1.4 V vs RHE. The voltammogram of the Pt/VC/N is also included for comparison (dotted lines). A blank run was also made without Pt. It was found from CV that the oxygen reduction current for the AC/N nanocomposite film without Pt NP decreased rapidly after a few potential cycles and therefore before each experimental run potential cycling was carried out in the window 0.0 V and +1.0 V vs RHE repeatedly for 10 times. This nullified the effect of the blank run and eliminates the need for subtracting the blank value from each experimental run. CVs were reproducible in the consecutive scans, and the voltammetry curves remained stable, confirming that during the experiment there was no dissolution of the components of the nanocomposite film. Though the voltammograms resemble that of polycrystalline Pt,[41] they lack the well-defined multiple peaks due to hydrogen adsorption in the cathodic sweep and its desorption in the reverse sweep like the characteristic CV pattern on Pt electrode in H_2SO_4 solution, which exhibits two peaks in the anodic branch from 0.0 V to +0.2 V vs RHE that are attributed to adsorption on different crystallographic planes of Pt.[42] In this study both the CVs of AC and VC support are almost similar with a single hydrogen adsorption and desorption peak indicating that Pt is present predominantly in a single crystallographic plane as confirmed by XRD. Also, the observation of peak currents of the hydrogen adsorption/desorption region indicates that surface properties of Pt/AC/N are similar to those of standard ORR catalyzing systems, namely, Pt/C or Pt/CNTs.[43] The platinum oxide formation wave at +1.15 V and its complete reduction at +0.6 V indicate the unique features of active surface Pt. But, the reduction current for VC supported Pt is less than that of AC supported Pt. The limiting current density obtained is comparable to some of the reported systems on Pt.[44−47] The ECSA was obtained from the N_2 CV curve[48] (Figure 5a) by integrating the area under the H-desorption region, subtracting the double-layer charging current, and dividing the resulting columbic charge by 210 μC/cm^2. For different Pt loadings the hydrogen

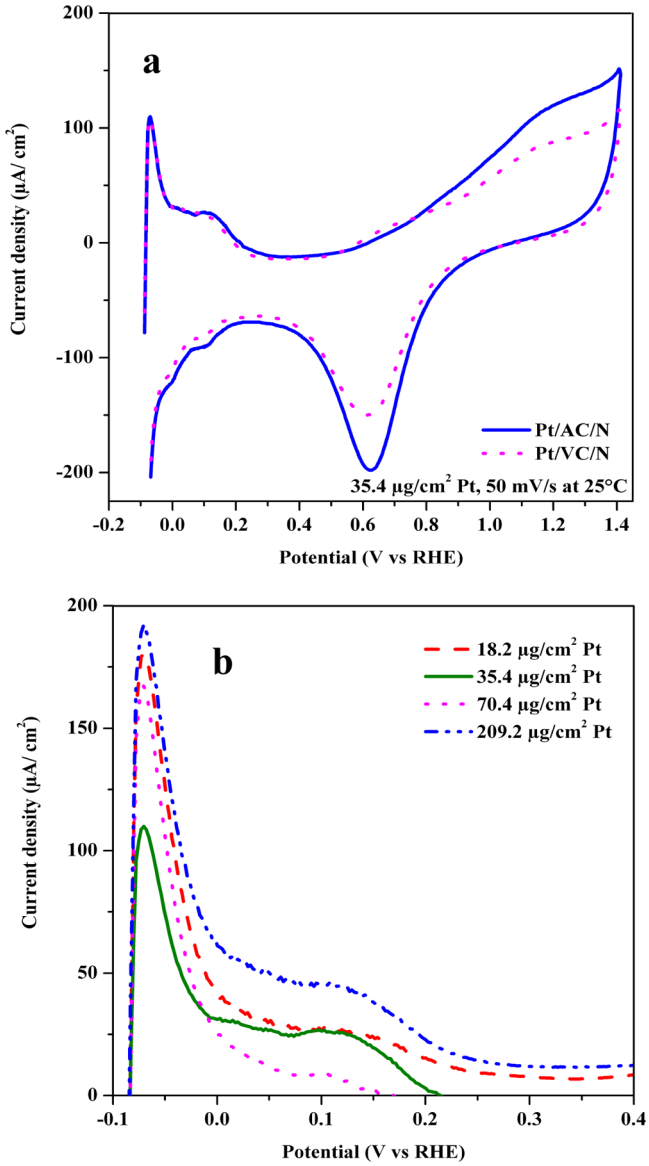

Figure 5. (a) CVs of clay and carbon supported Pt NP over Nafion matrix in N_2 saturated 0.5 M H_2SO_4 and (b) enhanced view of the H-desorption region for various Pt loadings supported on AC/Nafion taken from corresponding CVs in 0.5 M H_2SO_4 with N_2 purging.

desorption regions are shown in Figure 5b, and it can be seen that for the Pt mass loading of 35.4 μg/cm^2 the maximum current density was obtained with the calculated ECSA of 11.2 m^2/g. It is to be noted that though ECSA values are significant in finding the accessible surface area, the ORR activity does not always directly correspond to the measured surface area as evidenced from various literature reports (Supporting Information Table ST1). It can be observed from the Table ST1 that availability of ECSA alone does not ensure the extent of ORR activity, and there may be other influential parameters, namely, Pt−O coverage,[49] orientation of different crystallographic planes,[50] surface adsorption energy,[51] interfacial activity,[52] Pt−Pt interatomic distance,[53] and so forth, operating depending on the nature and type of the catalyst system, and as these parameters vary for different systems, there exists no linear correlation between ECSA and limiting current density. On the other hand, if the limiting current is divided by the actual Pt mass loading, the trend has now changed and

dx.doi.org/10.1021/am300697q | ACS Appl. Mater. Interfaces 2012, 4, 3620−3626

maximum current was seen for 18.2 $\mu g/cm^2$ (see the Supporting Information, SI-2).

The electrochemical reduction of oxygen on the electrocatalyst film was investigated in oxygen-saturated 0.5 M H_2SO_4 using a RRDE. Figure 6 presents the disk and ring currents in

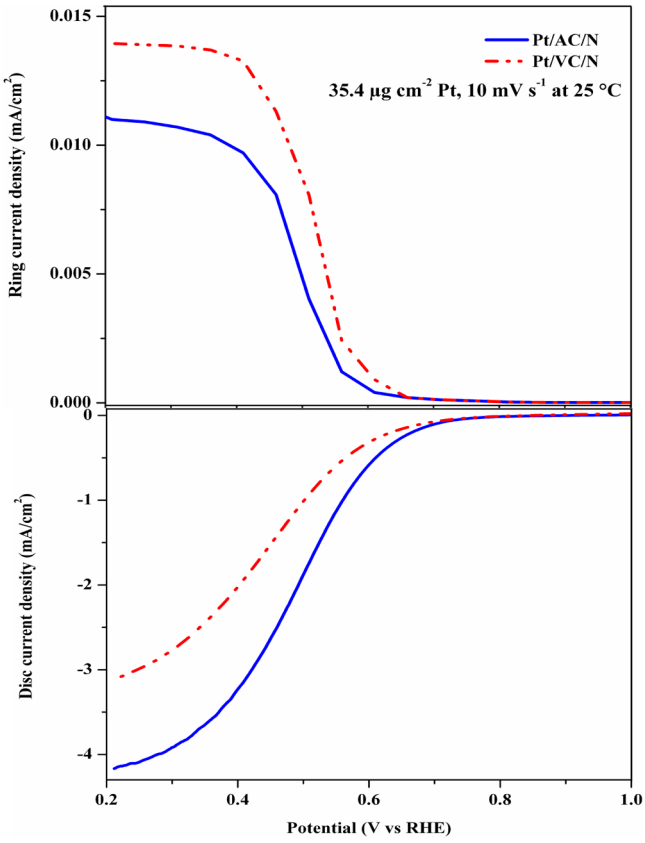

Figure 6. RRDE LSVs of 6 wt % AC and VC supported Pt NP over Nafion in O_2 saturated 0.5 M H_2SO_4 at 2000 rpm.

linear scan voltammogram (LSV) mode for Pt/VC/N and Pt/AC/N with 2000 rpm recorded at a 10 mV s^{-1} scan rate with the Pt mass loading of 35.4 $\mu g/cm^2$ at 25 °C. From the disk LSV curves three defined regions are observed: (i) kinetically controlled charge-transfer region from 0.91 to 0.65 V where the current density was not affected by the rate of mass transfer and is independent of the rotation rate; (ii) sloppy mixed kinetic and diffusion controlled region from 0.65 to 0.4 V, where the current is partially controlled by mass transport and partially by the kinetics of electron transfer; and (iii) diffusion/mass transfer controlled region also called limiting current region below 0.4 V. This sloppy increase in peak current from +0.65 to +0.4 V indicates the ORR current trend as reported elsewhere for Pt catalyst systems.[54−57] It can be seen from the RRDE disk currents (lower graph of Figure 6) that at 0.2 V the observed limiting current densities were 3.15 and 4.2 mA/cm^2, respectively, for VC and AC supports. The higher reduction current of Pt/AC/N than Pt/VC/N shows the improved catalytic activity of Pt supported on the AC/N matrix. On comparing the LSV limiting current of Pt/AC/N with commercial Pt/C systems (E-Tek), it was observed that Pt/AC/N possesses nearly equal or better ORR performance. In the reported commercial Pt/C systems, LSV currents ranged from 2.5 mA/cm^2 to 4.2 mA/cm^2, for Pt mass loadings of 40−170 $\mu g/cm^2$.[58−61] The onset potential taken from the Tafel plot (see the Supporting Information, SI-3) was found to be 0.91 V vs RHE for the Pt/AC/N film. On comparing the AC and VC, the onset potential for AC is 40 mV positively shifted, indicating early initiation of reduction kinetics. Nevertheless, compared to the standard Pt/C catalyst the onset potential of AC is less by 40 mV. The fact is that standard Pt/C catalysts are characterized by taking Pt/C catalyst slurry directly spread over the disk electrode and coating with a thin film of dilute Nafion as a binder material, whereas in this work Pt/AC/N nanocomposite was used as a catalyst film which might have contributed a higher diffusion resistance to the oxygen species and delayed the onset potential. From the disk and ring currents (Figure 6), the percentages of hydrogen peroxide were calculated.[37] It was observed that H_2O_2 formation was less at 2000 rpm and increased at lower rotation rates, and only a maximum of 1.6% H_2O_2 was formed, indicating a predominant four electron pathway.

Figure 7 shows the accelerated durability test LSV pattern observed at the 10th and 2000th potential cycles at the scan

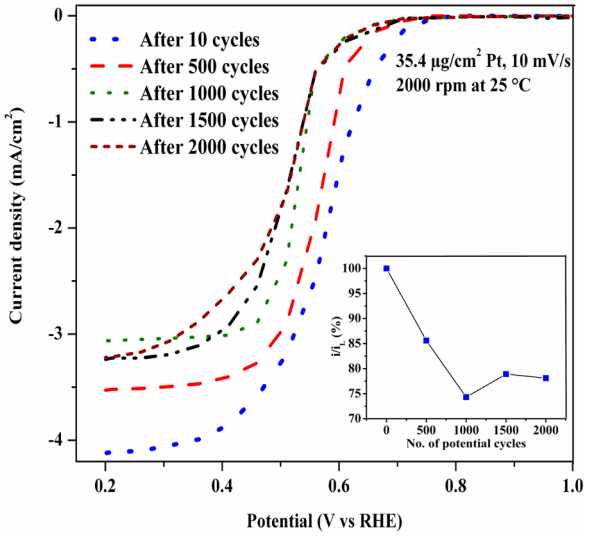

Figure 7. LSVs during ADT potential cycling of Pt/6 wt % AC/N nanocomposite in O_2 saturated 0.5 M H_2SO_4 at 25 °C (Inset: plot of i/i_L vs number of potential cycles).

rate of 10 mV/s and at 2000 rpm. The plot of observed limiting current with respect to the tenth cycle (i/i_L) vs number of potential cycles is given in the inset of Figure 7. Although during the first 1000 cycles a decreasing trend in limiting current was noted, it improved after 1000 cycles, and after 2000 cycles only ∼22% of limiting current loss was observed, as shown in the inset of Figure 7, and this trend might be due to the self-regeneration and surface activation of the initially blocked Pt surface as a result of electrochemical polishing during potential cycling. Under the fuel cell conditions (80 °C), nearly the same trend upon cycling was observed and affirms the potential possibility of Pt/AC/N catalyst film for practical utilization. It has been reported by Haung et al. that for Pt/C (50 wt % on TKK) catalyzed ORR in sulfuric acid medium the initial limiting current decreased ∼86% after 1500 cycles,[62] and this decrease is nearly four times higher than that of Pt/AC/N composite film catalyzed ORR. The chronoamperometric measurements of the two supports indicate that the corrosion current for the Pt/AC/N is nearly six times less than Pt/VC/N (Figure 8). This might be due to the lower poisoning of the Pt

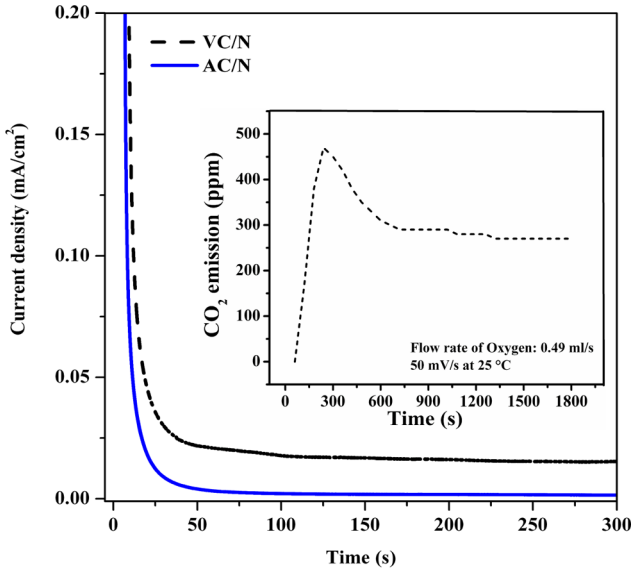

Figure 8. Chronoamperometric curves for AC and VC based Nafion nanocomposites in O_2 saturated 0.5 M H_2SO_4 at 25 °C at 0.7 V vs RHE (Inset: CO_2 evolution profile for the VC/N nanocomposite).

surface when embedded on AC compared to VC support. The real time CO_2 gas evolved during ORR in the case of Pt/VC/N was measured and is shown in the inset of Figure 8, and no such evolution was observed for Pt/AC/N. Hence, it can be said that AC exhibits better electrochemical stability as a support material compared to VC support for anchoring Pt NP. Instead of drop casting the nanocomposite slurry on the working electrode, separate free-standing films (thickness ~ 40 μm) were also cast over a Petri dish, peeled off, and recasted over the working electrode using a dilute Nafion solution as the binder. It was observed that, in both the cases, the current response was nearly the same, suggesting the possible use of the free-standing Pt/AC/N nanocomposite film for catalyzing the ORR in acid medium.

4. CONCLUSION

A novel synthetic "amino functionalized clay/Nafion" nanocomposite embedded with Pt NP was prepared. Pt NPs of the size < 5 nm are finely dispersed over AC/N matrix. The catalytic activity toward oxygen reduction reaction in 0.5 M H_2SO_4 was probed using CV and LSV under static and hydrodynamic conditions, respectively. From the RRDE ring and disk currents the maximum percentage of H_2O_2 intermediate formation was found to be ca. 1.6%. The nanocomposite showed good stability during potential cycling, and ca. 78% of the initial LSV current was retained at the end of 2000 cycles, indicating that Pt/AC/N is having significant stability in the acid environment for catalyzing ORR. Both the drop-casted and free-standing films (of thickness ~ 40 μm) were responding to the same extent toward ORR, hinting the possibility of using the nanocomposite film in small and portable PEM fuel cells as an electrocatalyst layer.

■ ASSOCIATED CONTENT

Supporting Information

ATR-FTIR spectra for pure aminoclay and Pt/AC/N nanocomposite, comparative current density curves with respect to Pt loading, Tafel plots for Pt/AC/N and Pt/VC/N, and a table containing the electrochemical surface area and ORR limiting current density data from various literature reports. This material is available free of charge via the Internet at http://pubs.acs.org.

■ AUTHOR INFORMATION

Corresponding Author

*E-mail: prof.balaji13@gmail.com.

Notes

The authors declare no competing financial interest.

■ ACKNOWLEDGMENTS

This work was financially supported by the Board of Research in Nuclear Sciences (BRNS), Department of Atomic Energy (DAE), Govt. of India, under Basic Sciences program through Sanction No. 2009/37/29/BRNS. S.B. thanks JNCASR, Bangalore, for the award of visiting scientist fellowship and profoundly thanks the management of SCSVMV University for having funded and created the necessary laboratory facilities to carry out this research project. B.N. thanks the BRNS for the award of Junior Research Fellowship (JRF). XRD, TGA, and TEM results obtained at the JNCASR are gratefully acknowledged.

■ REFERENCES

(1) Steele, B. C. H.; Heinzel, A. *Nature* **2001**, *414*, 345−352.
(2) Carrette, L.; Friedrich, K. A.; Stimming, U. *Fuel Cells* **2001**, *1*, 5−39.
(3) Hoogers, G. *Fuel cell technology handbook*; CRC Press: Boca Raton, FL, 2003; p 15.
(4) Litster, S.; McLean, G. *J. Power Sources* **2004**, *130*, 61−76.
(5) Kordesch, K.; Simader, G. *Fuel Cells and Their Applications*; VCH: New York, 1996; p 48.
(6) Service, R. F. *Science* **2002**, *296*, 1222−1224.
(7) Bruijn, F. D. *Green Chem.* **2005**, *7*, 132−150.
(8) Winter, U.; Herrmann, M. *Fuel Cells* **2003**, *3*, 141−145.
(9) Buchi, F. N.; Freunberger, S. A.; Reum, M.; Paganelli, G.; Tsukada, A.; Dietrich, P.; Delfino, A. *Fuel cells* **2007**, *7*, 159−164.
(10) Wang, Y.; Chen, K. S.; Mishler, J.; Cho, S. C.; Adroher, X. C. *Appl. Energy* **2011**, *88*, 981−1007.
(11) Shao, M. H.; Liu, P.; Adzic, R. R. *J. Am. Chem. Soc.* **2006**, *128*, 7408−7409.
(12) Wang, Y.; Balbuena, P. B. *J. Phys. Chem. B* **2004**, *108*, 4376−4384.
(13) Sun, S.; Zhang, G.; Geng, D.; Chen, Y.; Li, R.; Cai, M.; Sun, X. *Angew. Chem., Int. Ed.* **2011**, *50*, 422−426.
(14) Zhang, J.; Sasaki, K.; Sutter, E.; Adzic, R. R. *Science* **2007**, *315*, 220−222.
(15) Su, F.; Poh, C. K.; Tian, Z.; Xu, G.; Koh, G.; Wang, Z.; Liu, Z.; Lin, J. *Energy Fuels* **2010**, *24*, 3727−3732.
(16) Xu, F.; Wang, M.; Sun, H.; Simonson, S.; Ogbeifun, N.; Stach, E. A.; Xie, J. *J. Electrochem. Soc.* **2010**, *157*, B1138−B1145.
(17) Li, W.; Wang, X.; Chen, Z.; Waje, M.; Yan, Y. *Langmuir* **2005**, *21*, 9386−9389.
(18) Wang, X.; Li, W.; Chen, Z.; Waje, M.; Yan, Y. *J. Power Sources* **2006**, *158*, 154−159.
(19) Avasarala, B.; Moore, R.; Halder, P. *Electrochim. Acta* **2010**, *55*, 4765−4771.
(20) Sahu, A. K.; Pitchumani, S.; Sridhar, P.; Shukla, A. K. *Bull. Mater. Sci.* **2009**, *32*, 285−294.
(21) Mura, F.; Silva, R. F.; Pozio, A. *Electrochim. Acta* **2007**, *52*, 5824−5828.
(22) Zhang, W.; Li, M. K. S.; Yue, P. L.; Gao, P. *Langmuir* **2008**, *24*, 2663−2670.
(23) Premkumar, J.; Ramaraj, R. *J. Solid State Electrochem.* **1997**, *1*, 172−179.

(24) Thomassin, J. M.; Pagnoulle, C.; Bizzari, D.; Caldarella, G.; Germain, A.; Jerome, R. *Solid State Ionics* **2006**, *177*, 1137−1144.
(25) Burgaz, E.; Lian, H.; Alonso, R. H.; Estevez, L.; Kelarakis, A.; Giannelis, E. P. *Polymer* **2009**, *50*, 2384−2392.
(26) Bebin, P.; Caravanier, M.; Galiano, H. *J. Membr. Sci.* **2006**, *278*, 35−42.
(27) Mishra, A. K.; Kuila, T.; Kim, N. H.; Lee, J. H. *J. Membr. Sci.* **2012**, *389*, 316−323.
(28) Jung, D. H.; Choa, S. Y.; Pecka, D. H.; Shina, D. R.; Kim, J. S. *J. Power Sources* **2003**, *118*, 205−211.
(29) Ahmad, M. B.; Hoidy, W. H.; Bt Ibrahim, N. A.; Jaffar Al-Mulla, E. A. J. *Eng. Appl. Sci.* **2009**, *4*, 184−188.
(30) Xiuchong, H.; Haolin, T.; Mu, P. *J. Appl. Polym. Sci.* **2008**, *108*, 529−534.
(31) Alonso, R. H.; Estevez, L.; Lian, H.; Kelarakis, A.; Giannelis, E. P. *Polymer* **2009**, *50*, 2402−2410.
(32) Mauritz, K. A.; Moore, R. B. *Chem. Rev.* **2004**, *104*, 4535−4585.
(33) Datta, K. K. R.; Eswaramoorthy, M.; Rao, C. N. R. *J. Mater. Chem.* **2007**, *17*, 613−615.
(34) Datta, K. K. R.; Kulkarni, C.; Eswaramoorthy, M. *Chem. Commun.* **2010**, *46*, 616−618.
(35) Johnsy, G.; Datta, K. K. R.; Sajeevkumar, V. A.; Sabapathy, S. N.; Bawa, A. S.; Eswaramoorthy, M. *ACS Appl. Mater. Interfaces* **2009**, *1*, 2796−2803.
(36) Whilton, N. T.; Burkett, S. L.; Mann, S. *J. Mater. Chem.* **1998**, *8*, 1927−1932.
(37) Lefevre, M.; Dodelet, J. P. *Electrochim. Acta* **2003**, *48*, 2749−60.
(38) Technical Note 2005-01; Pine Research Instrumentation, 2007. http://www.pineinst.com/echem/files/LMECN200501.pdf.
(39) Patil, A. J.; Muthusamy, E.; Mann, S. *Angew. Chem., Int. Ed.* **2004**, *43*, 4928−4933.
(40) Barbora, L.; Acharya, S.; Singh, R.; Scott, K.; Verma, A. *J. Membr. Sci.* **2009**, *326*, 721−726.
(41) Bard, A. J.; Faulkner, L. R. *Electrochemical Methods, Fundamentals and Applications*, 2nd ed.; John Wiley: New York, 2001; p 560.
(42) Sawyer, D. T.; Sobkwiak, A.; Roberts, J. L. *Electrochemistry for chemists*, 2nd ed.; John Wiley: New York, 1995; p 217.
(43) Pang, M.; Li, C.; Ding, L.; Zhang, J.; Su, D.; Li, W.; Liang, C. *Ind. Eng. Chem. Res.* **2010**, *49*, 4169−4174.
(44) Yano, H.; Higuchi, E.; Uchida, H.; Watanabe, M. *J. Phys. Chem. B* **2006**, *110*, 16544−16549.
(45) Arruda, T. M.; Shyam, B.; Ziegelbauer, J. M.; Mukerjee, S.; Ramaker, D. E. *J. Phys. Chem. C* **2008**, *112*, 18087−18097.
(46) Peng, Z.; Wum, J.; Yang, H. *Chem. Mater.* **2010**, *22*, 1098−1106.
(47) Kou, R.; Shao, Y.; Wang, D.; Engelhard, M. H.; Kwak, J. H.; Wang, J.; Viswanathan, V. V.; Wang, C.; Lin, Y.; Wang, Y.; Aksay, I. A.; Liu, J. *Electrochem. Commun.* **2009**, *11*, 954−957.
(48) Carmoa, M.; Santo, A. R. D.; Poco, J. G. R.; Linardi, M. *J. Power Sources* **2007**, *173*, 860−866.
(49) Zhang, J.; Lima, F. H. B.; Shao, M. H.; Sasaki, K.; Wang, J. X.; Hanson, J.; Adzic, R. R. *J. Phys. Chem. B* **2005**, *109*, 22701−22704.
(50) Lee, S. W.; Chen, S.; Suntivich, J.; Sasaki, K.; Adzic, R. R.; Horn, Y. S. *J. Phys. Chem. Lett.* **2010**, *1*, 1316−1320.
(51) Teliska, M.; Murthi, V. S.; Mukerjee, S.; Ramaker, D. E. *J. Phys. Chem. C* **2007**, *111*, 9267−9274.
(52) Subbaraman, R.; Strmcnik, D.; Paulikas, A. P.; Stamenkovic, V. R.; Markovic, N. M. *Chem. Phys. Chem.* **2010**, *11*, 2825−2833.
(53) Jalan, V.; Taylor, E. J. *J. Electrochem. Soc.* **1983**, *130*, 2299−2301.
(54) Chen, W.; Kim, J.; Sun, S.; Chen, S. *J. Phys. Chem. C* **2008**, *112*, 3891−3898.
(55) Jeyabharathi, C.; Mathiyarasu, J.; Phani, K. L. N. *J. Appl. Electrochem.* **2009**, *39*, 45−53.
(56) Kuzume, A.; Herrero, E.; Feliu, J. M. *J. Electroanal. Chem.* **2007**, *599*, 333−343.
(57) Alcantara, K. S.; Feria, O. S. *Fuel Cells* **2010**, *10*, 84−92.
(58) Chen, Z.; Waje, M.; Li, W.; Yan, Y. *Angew. Chem.* **2007**, *119*, 4138−4141.
(59) Jeyabharathi, C.; Venkateshkumar, P.; Mathiyarasu, J.; Phani, K. L. N. *Electrochim. Acta* **2008**, *54*, 448−454.
(60) Song, S.; Wang, Y.; Tsiakaras, P.; Shen, P. K. *Appl. Catal., B* **2008**, *78*, 381−387.
(61) Liu, L.; Lee, J. W.; Popov, B. N. *J. Power Sources* **2006**, *162*, 1099−1103.
(62) Huang, S. Y.; Ganesan, P.; Popov, B. N. *ACS Catal.* **2012**, *2*, 825−831.